Dynamics of space-time self-focusing of a femtosecond relativistic laser pulse in an underdense plasma

Maurizio Lontano[1] and Ivane G. Murusidze[2]
[1]*Istituto di Fisica del Plasma, Consiglio Nazionale delle Ricerche, 20125 Milano, Italy*
[2]*Institute of Physics, Georgian Academy of Sciences, 370077 Tbilisi, Georgia*
lontano@ifp.cnr.it, miv_laser@gol.ge

Abstract: The propagation of femtosecond, multiterawatt, relativistic laser pulses in a transparent plasma is studied. The spatio-temporal dynamics of ultrashort, high-power laser pulses in underdense plasmas differs dramatically from that of long laser beams. We present the results of numerical studies of these dynamics within a model which systematically incorporates finite pulse length effects (*i.e.*, dispersion) along with diffraction and nonlinear refraction in a strongly nonlinear, relativistic regime. New space-time patterns of self-compression, self-focusing and self-phase-modulation, typical of ultrashort, high-intensity laser pulses, are analyzed. The parameters of our numerical simulations correspond to a new class of high-peak-power (> 100 TW), ultrashort-pulsed laser systems, producing pulses with a duration in the 10 – 20 femtosecond range. Spatio-temporal dynamics of these self-effects and underlying physical mechanisms are discussed.

OCIS codes: (190.5530) Pulse propagation and solitons; (190.5940) Self-action effects; (260.5950) Self-focusing; (350.5400) Plasmas

References

1. M. D. Perry and G. Mourou, "Terawatt to petawatt subpicosecond lasers," Science **64**, 917-924 (1994).
2. G. A. Mourou, C. P. J. Barty and M. D. Perry, "Ultrahigh-Intensity Lasers: Physics of the Extreme on a Tabletop," Phys. Today **51**, 22-28 (1998).
3. K. Yamakawa, M. Aoyama, T. Kase, Y. Akahane, and, H. Takuma, "100-TW sub-20-fs Ti:sapphire laser system operating at a 10-Hz repetition rate," Opt. Lett. **23**, 1468-1470 (1998).
4. K. Yamakawa, C. P. J. Barty, "Ultrafast, ultrahigh-peak, and high-average power Ti:sapphire laser system and its application", IEEE J. Se. Top. Quantum Electron. **6**, 658-675 (2000).
5. K. Yamakawa, Y. Akahane, M. Aoyama, Y. Fukuda, N. Inoue, J. Ma, and H. Ueda, "Status and future developments of ultrahigh intensity lasers at JAERI," in *Superstrong Fields in Plasmas*, M. Lontano, G. Mourou, O. Svelto, T. Tajima, eds., AIP Conference Proceedings, Vol.611 (American Institute of Physics, Melville, New York, 2002), pp. 385-396.
6. T. Tajima and G. Mourou, "Superstrong field science," *ibid*. pp. 423-436.
7. P. Sprangle, C.-M. Tang, E. Esarey, "Relativistic self-focusing of short-pulse radiation beams in plasmas," IEEE Trans. Plasma Sci. **PS-15**, 145-153 (1987).
8. G.-Z. Sun, E. Ott, Y. C. Lee, and P. Guzdar, "Self-focusing of short intense pulses in plasmas," Phys. Fluids **30**, 526-532 (1987).
9. E. Esarey, P. Sprangle, J. Krall, A. Ting, "Self-focusing and guiding of short laser pulses in ionizing gases and plasmas," IEEE J. Quantum Electron. **33**, 1879-1914 (1997).
10. W. B. Mori, "The physics of the nonlinear optics of plasmas at relativistic intensities for short-pulse lasers," IEEE J. Quantum Electron. **33**, 1942-1953 (1997).
11. B. Hafizi, A. Ting, P. Sprangle, and R. F. Hubbard, "Relativistic focusing and ponderomotive channeling of intense laser beams," Phys. Rev. E **62**, 4120-4125 (2000).
12. P. Spangle, B. Hafizi, and J. R. Peñano, "Laser pulse modulation instabilities in plasma channels," Phys. Rev. E **61**, 4381-4393 (2000).

#1991 - $15.00 US Received December 23, 2002; Revised February 04, 2003

13. E. Esarey, C. B. Schroeder, B. A. Shadwick, J. S. Wurtele, and W. P. Leemans, **"**Nonlinear Theory of Nonparaxial Laser Pulse Propagation in Plasma Channels," Phys. Rev. Lett. **84**, 3081-3084 (2000).
14. S. V. Bulanov, I. N. Inovenkov, V. I. Kirsanov, N. M. Naumova, and A. S. Sakharov, "Nonlinear depletion of ultrashort and relativistically strong laser pulses in an underdense plasma, " Phys. Fluids B **4**, 1935-1942 (1992) .
15. D. Farina, M. Lontano, I. G. Murusidze, S. V. Mikeladze, "Hydrodynamic approach to the interaction of a relativistic ultrashort laser pulse with an underdense plasma," Phys. Rev. E **63**, 056409(10) (2001).
16. I. G. Murusidze, G. I. Suramlishvili, M. Lontano, "Spatiotemporal self-focusing and splitting of a femtosecond, multiterawatt, relativistic laser pulse in an underdense plasma," in *Superstrong Fields in Plasmas*, M. Lontano, G. Mourou, O. Svelto, T. Tajima, eds., AIP Conference Proceedings, Vol.611 (American Institute of Physics, Melville, New York, 2002), pp. 177-184.
17. A. E. Siegman, *Lasers* (University Science Books, Mill Valley, CA, 1986).
18. T. Brabec and F. Krausz, "Nonlinear Optical Pulse Propagation in the Single-Cycle Regime," Phys. Rev. Lett. **78**, 3282-3285 (1997).
19. I. G. Murusidze, L. N. Tsintsadze, "Generation of large amplitude plasma wakefields with low phase velocities by an intense short laser pulse," J. Plasma Phys. **48**, 391-395 (1992).
20. S. A. Akhmanov, V. A. Vysloukh, and A. S. Chirkin, *Optics of Femtosecond Laser Pulses* (AIP, New York, 1992).
21. R. Trebino, K. W. DeLong, D. N. Fittinghoff, J. N. Sweetser, M. A. Krumbügel, B. A. Richman, D. J. Kane "Measuring ultrashort laser pulses in the time-frequency domain using frequency-resolved optical gating," Rev. Sci. Inst. **68**, 3277-3295 (1997).
22. I. Watts, M. Zepf, E. L. Clark, M. Tatarakis, K. Krushelnik, A. E. Dangor, R Alott, R. J. Clarke, D. Neely, P. N. Norreys, "Measurement of relativistic self-phase-modulation in plasma," Phys. Rev. E **66**, 036409 (2002).

1. Introduction

The progress in developing ultrashort-pulse laser sources, based on the technique of chirped pulse amplification (CPA) [1,2], has made available high peak power (from multiterawatt to petawatt) laser pulses on a femtosecond time scale. A compact CPA laser system produces pulses with peak powers in excess of 100 TW and durations less than 19 fs [3]. The same ultrafast CPA architecture enables production of optical pulses with petawatt peak powers. With increasing peak powers, pulse durations have been steadily decreased and now high peak power CPA systems are evolving into the 10-fs range [4,5]. Such systems have made available pulses with peak intensities in the 10^{20} W/cm^2 range, and, in the near future, it is expected to increase by at least two orders of magnitude [6]. At these intensities, the electron motion in the laser fields becomes highly relativistic and nonlinear. These recent achievements are bringing the nonlinear optics of laser pulses in plasmas to a new physical regime of laser-plasma interactions, dominated by (i) strong relativistic nonlinearities and (ii) finite-pulse-length effects.

The propagation dynamics of intense laser beams through underdense plasmas have been studied intensively, as it is of topical interest for developing laser-plasma accelerators, new plasma based x-ray sources and several other applications [6-12]. These studies have mostly dealt with the evolution of finite-radius, tightly focused, relatively long (on picosecond or sub-picosecond time scales) laser pulses, often at weakly relativistic intensities. In this regime of propagation the pulse evolution is governed by diffraction and nonlinear refraction effects. Consequently, relevant theoretical models are usually based on the paraxial wave equation containing diffraction and nonlinear refraction terms, but neglecting finite pulse duration (*i.e.*, dispersion) effects. Therefore this approach is incapable of describing the evolution of the pulse's temporal profile as well as related propagation effects, which become essential for the ultrashort pulse dynamics. However, recent works show that even the behavior of relatively long laser pulses, for which dispersion effects are only corrections to the dominant diffraction and nonlinear refraction effects, may be affected considerably over long propagation distances [12,13].

#1991 - $15.00 US Received December 23, 2002; Revised February 04, 2003

In this paper we study the propagation dynamics of laser pulses within the parameter regime corresponding to a new class of compact, high-power, ultrashort pulsed laser systems, producing pulses in the 10-20 fs range [3,5]. For such pulses, the conventional paraxial approach is no longer an adequate description. In the next section we formulate an adequate model which extends the conventional paraxial wave equation, systematically incorporating all relevant finite-pulse-length effects. Within this model we are able to describe the evolution of wide, loosely focused, ultrashort-duration relativistic laser pulses in the regime of parameters, when dispersion contributes equally along with diffraction and nonlinear refraction in the pulse evolution. Fully relativistic formulation of the governing wave and plasma response equations also enables one to consider pulses with arbitrary high intensities. The nonlinear evolution of a one-dimensional ultrashort, relativistically intense laser pulse propagating in an underdense plasma has been studied in [14]. The numerical simulations presented here, based on a three-dimensional hydrodynamic model, reveal new self-focusing (SF), self-compression (SC) and self-phase-modulation (SPM) patterns, typical of ultrashort, relativistic laser pulses only, which provide an evidence of strong coupling between temporal and spatial evolution of the pulse. In Section 2 we describe the physical model. The results of the numerical simulations and their detailed discussion are given in Section 3.

2. Physical model

Our studies of the propagation of ultrashort, ultraintense laser pulses through an underdense plasma is based on a model which systematically incorporates finite-pulse-length effects (*i.e.*, dispersion) self-consistently with diffraction and noninlinear refraction. The detailed derivation of the basic equations is given in [15]. Here we outline the principal relations and conditions, on which the model is based. Thus this model is aimed at describing laser pulses, for which dispersion effects play as important a role as diffraction. Such regime of propagation in underdense plasmas, where the ratio of the plasma frequency to the (central) laser frequency, $\omega_p/\omega << 1$, is a small parameter, naturally implies a pulse whose effective length ℓ_{L} is much less than its width, $\ell_{\mathrm{L}} << \ell_{\perp}$, where $\ell_{\perp}$ scales its transverse (to the propagation direction) dimension. Indeed, when the characteristic diffraction length of an optical pulse, $L_{\mathrm{dif}} = k\ell_{\perp}^2$, where k is the wavenumber corresponding to ω, is comparable to its dispersion length $L_{\mathrm{disp}} = (\omega/\omega_p)^2 k\ell_{\mathrm{L}}^2$, i.e., $L_{\mathrm{dif}} \approx L_{\mathrm{disp}}$, then $(\ell_{\mathrm{L}}/\ell_{\perp})^2 \approx (\omega_p/\omega)^2 << 1$. In addition, a pulse with duration on a femtosecond time scale, for $\lambda \approx 1$ μm radiation, will contain a few optical cycles, which makes it necessary to take into account also the first-order dispersion effects. Thus we have the following scalings

$$\ell_{\mathrm{L}}/\ell_{\perp} \sim \ell_{\perp}/\ell_{\parallel} \sim \omega_p/\omega \equiv \varepsilon << 1, \tag{1}$$

where $\ell_{\parallel}$ is the length scale over which the laser pulse changes significantly due to propagation effects (diffraction, dispersion and nonlinear refraction). According to these scalings the laser pulse may be identified as a thin, wide disk of light with a sharp intensity gradient along the propagation direction and a smooth transverse profile.

The plasma is modeled by the relativistic fluid equations for cold electrons. This model gives an adequate description of plasmas within the assumptions that, first, the laser pulse duration is short enough and therefore the ions are assumed to be virtually immobile during the transit of the ultrashort pulse, and, second, it is also assumed that, at relativistic intensities, the electrons are driven to velocities much higher than their thermal velocities.

Within the regime of parameters outlined above, we model the evolution of the circularly polarized laser pulse propagating in the z direction and described by the transverse component of its vector potential

$$\mathbf{A} = \frac{1}{2}(\mathbf{x} \pm i\mathbf{y})A(\mathbf{r},t)\exp(ikz - i\omega t) + c.c., \tag{2}$$

#1991 - $15.00 US Received December 23, 2002; Revised February 04, 2003

where $A(\mathbf{r},t)$ is the pulse envelope, generally a complex valued function, ω is the central frequency, and k is the corresponding wavenumber in the plasma, $kc = \omega(1-(\omega_p^2/\omega^2))^{1/2}$.

From Maxwell's equations and the relativistic electron fluid equations to the lowest (zeroth-order) in the small parameter ε we derive the following set of coupled equations [15,16]

$$2ik\frac{\partial A}{\partial \zeta} - \frac{2}{v_g}\frac{\partial^2 A}{\partial \tau \partial \zeta} - d\frac{\partial^2 A}{\partial \tau^2} + \nabla_\perp^2 A =$$

$$k_p^2\left(\frac{\beta_g}{\left[(1+\varphi)^2 - (1+|A|^2)/\gamma_g^2\right]^{1/2}} - 1\right)A, \tag{3}$$

$$\frac{\partial^2 \varphi}{\partial \tau^2} = \omega_p^2(\beta_g\gamma_g)^2\left(\frac{\beta_g(1+\varphi)}{\left[(1+\varphi)^2 - (1+|A|^2)/\gamma_g^2\right]^{1/2}} - 1\right). \tag{4}$$

Here we have employed a moving frame of reference introducing the variables $\zeta = z$, $\tau = t - z/v_g$, where $v_g \equiv \partial\omega/\partial k = kc^2/\omega$ is the group velocity, $\beta_g = v_g/c$, $\gamma_g = (1-\beta_g^2)^{-1/2}$. Note that, independent variables in Eqs. (3)-(4) are dimensional, whereas $A \to eA/(mc^2)$, and $\varphi \to e\varphi/(mc^2)$ (scalar potential) refer to the dimensionless quantities throughout the paper.

Equation (3) is the wave equation, which governs the evolution of the envelope $A(\mathbf{r}_\perp, \zeta, \tau)$ of the ultrashort, relativistically intense laser pulse propagating in an underdense plasma. The second and the third terms on its left-hand side account for finite pulse duration. They represent the first- and second-order dispersion effects, respectively. The coefficient of the third term, $d = k\partial^2 k/\partial\omega^2 = -(k/v_g^2)\partial v_g/\partial\omega$, is proportional to the group-velocity dispersion parameter. In our case $d = -v_g^{-2}(\omega_p/\omega)^2$, i.e., the third term in Eq. (3) accounts for negative or "anomalous" GVD, as is typical of transparent plasmas. The fourth term is the diffraction term. The only term neglected on the left of Eq. (3) is the term $\partial_{\zeta\zeta}^2 A$, which is second-order in ε, i.e., the conventional paraxial approximation [17] is naturally assumed within the parameter regime outlined by Eq. (1): $k^{-1} << \ell_\perp << \ell_\parallel \sim k\ell_\perp^2$. In addition, under the same conditions, the GVD and the diffraction terms contribute equally in the pulse evolution. The first order dispersion (FOD) term extends the applicability of Eq. (3) down to single-cycle pulses. Note that the phase in Eq. (2) $\phi_0 = kz - \omega t$ varies slowly with ζ. Indeed in our case $|\partial_\zeta \phi_0| = |(v_g - v_\phi)/v_g|\, k = \beta_g^{-2}\varepsilon^2 k << k$, which is also one of the prerequisites for a consistent extension of the wave equation down to single-cycle regime [18].

Incorporating all relevant finite-pulse-length effects within the paraxial approximation, the wave equation, Eq. (3), will be referred to as the pulsed paraxial wave equation (PPWE). In the sense used by us in [15,16] and followed here, the PPWE is an extension of the classical paraxial wave equation designed first for light beams–infinite-length light pulses. Thus within the PPWE we are able to describe ultrashort pulses propagating in underdense plasmas in the regime when dispersion and diffraction effects play an equally important role.

The terms contributing to the nonlinear refraction are on the right-hand side of Eq. (3). It is expressed through the scalar and vector potentials and contains contributions both from the relativistic mass increase of the electrons and from the electron density perturbations due to ponderomotive action of the laser pulse. It is valid for arbitrary large values of A as well as φ, thus giving fully relativistic description of the refractive index at relativistic intensities of the propagating pulse.

#1991 - $15.00 US Received December 23, 2002; Revised February 04, 2003

Equation (4), describing the dynamic plasma response to the laser pulse, is the Poisson's equation, the right hand-side of which is expressed in terms of the vector and scalar potentials. The scalar potential, φ, accounts for the electrostatic field, which results from electron density perturbations ponderomotively driven by the laser pulse. Integrating the leading-order (zeroth-order in ε) fluid equations, we derive the following relations $\beta_g p_z = \gamma - \varphi - 1$ and $n(\beta_g - p_z/\gamma) = \beta_g$, where p_z $(\rightarrow p_z/mc)$ is the normalized longitudinal momentum of the electrons, n $(\rightarrow n/n_0)$ is the electron density normalized to its unperturbed initial value, and the relativistic factor $\gamma = (1 + p_z^2 + |A|^2)^{1/2}$ [15]. At relativistic laser amplitudes, $|A| > 1$, the longitudinal momentum is also relativistic, and is on the order of the transverse momentum, i.e., $|p_z|_{\max} \sim |A|_{\max}$. Thus the relativistic axial motion of electrons ponderomotively excited by the laser pulse, equally with the transverse oscillations of the electrons in the laser field, contributes to the relativistic reduction (depression) of the local plasma frequency ($\omega_p \propto \gamma^{-1/2}$), hence, to the corresponding increase in the local refractive index [15]. The hierarchy of scales implied by Eq. (1) naturally leads to the plasma response, which is described self-consistently within the quasistatic approximation in the wide pulse limit ($k_p \ell_\perp >> 1$, where $k_p = \omega_p/c$) [15,19]. The equation for the plasma response is valid for arbitrarily large relativistic laser intensities, when the amplitude of the normalized vector potential of the laser field, the so-called laser strength parameter, $a_0 \equiv eA_0/(mc^2) > 1$, which implies $I\lambda^2 > \alpha_\Pi \cdot 1.37 \times 10^{18}$ W cm^{-2} μm^2 where I is the laser intensity and λ is the wavelength, and $\alpha_\Pi = 1, 2$ for linear and circular polarization, respectively. At these laser parameters the plasma response, in general, can be excited with relativistic amplitudes, *i.e.* $|\varphi| > 1$.

For the laser-plasma parameters within the range of our interest it is also typical that the laser pulse length is less than the plasma wavelength, λ_p, $\ell_L < \lambda_p$, *i.e.* our pulse is so short that it does not see even a single plasma wavelength. Therefore its coupling with plasma waves cannot be described in terms of the conventional wave-wave interaction. The shortness of the pulse can suppress parametric Raman processes and significantly limit the number of instabilities. However, the ultrashort pulse experiences a new type of instabilities, which are the subject of our studies in the following section.

3. Space-time self-focusing and splitting of laser pulse

In the numerical simulations, based on Eqs. (3)-(4), we model the propagation of an ultrashort, relativistically intense, circularly polarized laser pulse focused at the edge of a preformed underdense plasma. At the input plane $\zeta = 0$ the laser field is given by $A = A_0 \exp(-\tau^2/\tau_0^2 - r^2/w_0^2)$, where $r \equiv (x^2 + y^2)^{1/2}$, and the amplitude A_0 is a real constant. Having no initial phase varying with τ, the pulse is transform-limited [20], *i.e.* with no frequency modulation at the input plane. The radial dependence of the pulse corresponds to the fundamental Gaussian mode with a spot size w_0 and a planar wave front (with infinite radius of curvature) [17]. Though axial symmetry of the pulse's transverse profile is maintained during the entire time of the simulation evolution, however, in the course of the propagation the pulse develops transverse profiles with higher order axial symmetry as we go from the front to the back of the pulse. Simulation results described here represent a laser pulse with the following dimensionless parameters: the pulse amplitude $A_0 = 3$; the ratio of the laser spot size to the plasma skin depth $w_0 k_p = 25$; the ratio of the initial effective pulse duration to the spot size is defined by $v_g \tau_0 / w_0 = 0.1$. The preformed plasma is assumed to be underdense with $n/n_c = (\omega_p/\omega)^2 = 0.01$, where n_c is the critical plasma density. For $\lambda = 800$ nm laser wavelength, the above dimensionless parameters imply a laser pulse with a peak intensity $I_0 = 3.85 \times 10^{19}$ W/cm^2, peak power $P_0 = 612.7$ TW, spot size $w_0 = 31.8$ μm,

#1991 - $15.00 US Received December 23, 2002; Revised February 04, 2003

duration (length) $\tau_{\mathrm{FWHM}} = 12.6$ fs (3.77 μm) full width at half maximum of the intensity profile. The vacuum Rayleigh length for this pulse is $Z_R = 3.98$ mm. The plasma density $n = 1.74 \times 10^{19}$ cm^{-3} and the corresponding plasma wavelength $\lambda_p = 8\,\mu\mathrm{m}$ ($k_p^{-1} = 1.27\,\mu\mathrm{m}$). Note that the peak power is well above the critical power for relativistic self-focusing, which for our parameters is $P_{\mathrm{cr}} \approx 1.7$ TW [7,8]. The numerical method is based on a finite-difference scheme with first-order accuracy in ζ and second-order accuracy in τ, x, and y. Radiative (vanishing reflection coefficient) boundary conditions are applied [15]. It should be noted that we have simulated the laser propagation within this model for various laser and plasma

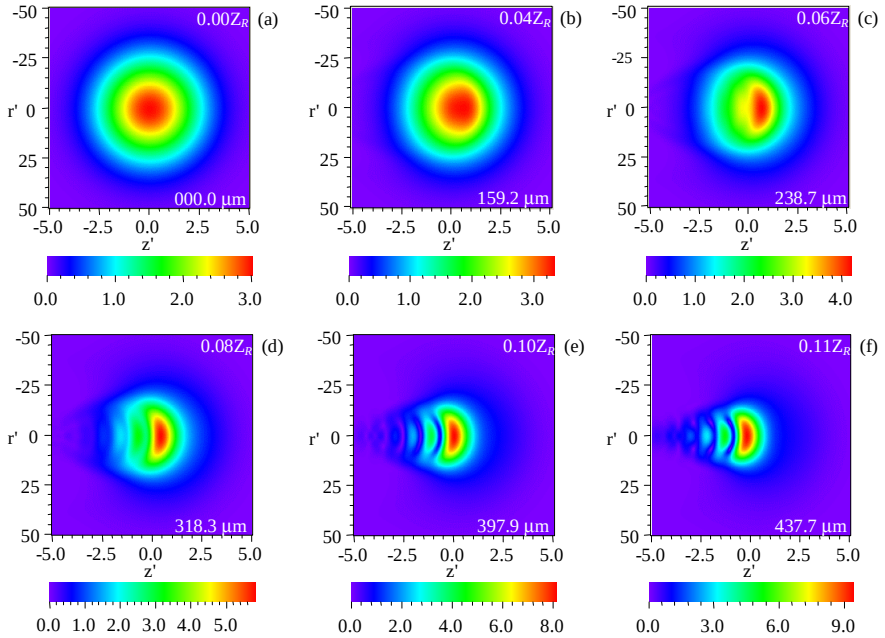

Fig. 1. The sequence of contour plots shows the evolution of the laser field amplitude $|A|$ (in mc^2/e units) during its propagation through an underdense plasma. The initial Gaussian pulse has $A_0 = 3$, $w_0 k_p = 25$, $k_p v_g \tau_0 = 2.5$. $|A|$ is mapped in (z', r') plane, where $z' = k_p(z - v_g t)$ and $r' = k_p r$ are the dimensionless longitudinal (in the moving frame) and radial coordinates in k_p^{-1} units, respectively. Propagation distances into the plasma are shown in the right upper and lower corners of each plot in units of the Rayleigh length and in micrometers, respectively.

parameters. The results presented here for the parameters discussed above typify the behavior and space-time patterns revealed in these simulations [16].

The sequence of contour plots in Fig. 1 shows the dynamics of the simultaneous SF and SC of the pulse and its subsequent splitting. Here $|A|$ is mapped in (z', r') plane, where $z' = k_p(z - v_g t)$ and $r' = k_p r$ are the dimensionless longitudinal (in the moving frame) and radial coordinates in k_p^{-1} units, respectively. Note that the scale of the r' axis is ten times larger than that of the z' axis. The propagation distances into the plasma are shown at the right upper and lower corners of each plot in units of the Rayleigh length and in micrometers, respectively. At the initial stage up to a propagation distance $\approx$160 μm ($0.04Z_R$) the pulse almost preserves its proportions in spite of the contraction of its radial and longitudinal dimensions due to SF and SC. A noticeable increase in the peak amplitude is already evident in Fig. 1(c). Here the pulse's peak is shifted forward and leading edge has become steeper. In the following stage modulations of both the longitudinal (time) and radial profiles become

#1991 - $15.00 US
Received December 23, 2002; Revised February 04, 2003

evident. At this stage the trailing half of the pulse develops noticeable modulations of the time profile which become well pronounced after propagating 318 μm ($0.08Z_R$), Fig. 1(d). Becoming deeper with the intensity dropping almost to zero between successive peaks, these modulations eventually lead to pulse splitting into a sequence of pulses, which follow each other arranged in decreasing order of their amplitudes, Fig. 1(e), 1(f). The initial stage of this splitting is shown also in Fig. 4(a), and the further dynamics of the time profile modulations is shown in Figs. 5(a) and 5(b). Eventually one can identify three separate peaks with relativistic amplitudes at the split back of the pulse.

The dynamics of the pulse's effective width and length with the propagation distance is shown in Fig. 2(a). Here $\underline{w}_{\text{eff}}$ is the radial variance [17] normalized to its initial value $w_0/\sqrt{2}$,

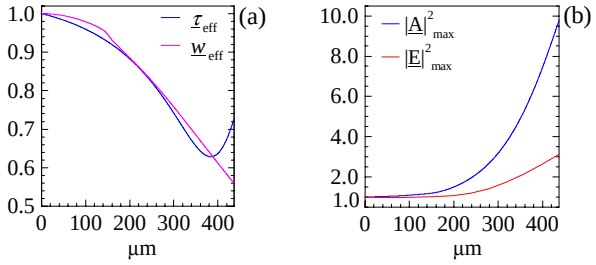

Fig. 2. (a) – The effective width $\underline{w}_{\text{eff}}$ and the effective duration $\underline{\tau}_{\text{eff}}$ of the laser pulse are shown vs. the propagation distance (in micrometers). Underlined quantities refer to their normalized values. (b) - Dynamics of the peak values of the squared amplitudes of the laser vector potential and of the electric field (normalized to their initial values) during the pulse propagation.

and $\underline{\tau}_{\text{eff}}$ is the root mean square (rms) duration [20] corresponding to the pulse's on-axis time profile normalized to its initial value, which for our input pulse is $\tau_0/2$. Figure 2(a) clearly illustrates that the rates of SF and SC remain very close to each other up to the time when the pulse has traveled 437.7 μm ($0.11Z_R$), thus the initial ratio of the pulse length to its width is preserved. Figure 2(b) shows the increase in the laser peak intensity $I \propto |E|^2_{\max}$ by a factor of three after the pulse has traveled ≈ 0.4 mm through the plasma, while $|A|^2_{\max}$ is increased almost by an order of magnitude. Such high rate of energy concentration is a result of the simultaneous SF and SC of the pulse. Note that $|E| \sim c^{-1}|(\omega+\delta\omega)||A|$, where $\delta\omega$ is the frequency shift associated with SPM induced phase shifts. Large frequency downshifts in the focal region, which will be analyzed below, explain the difference between the growth rates.

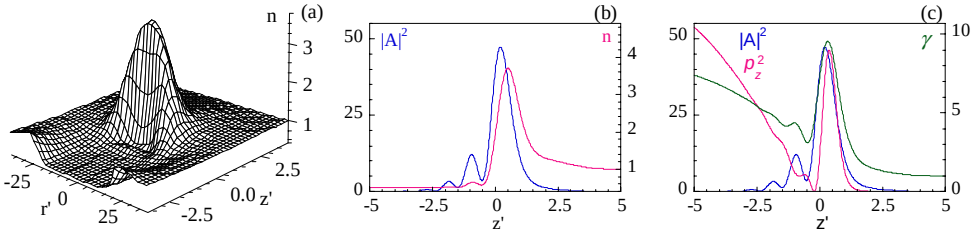

Fig. 3. The axial (longitudinal) asymmetry of the plasma response is illustrated. (a) – Surface plot of the electron density within the focal region. The corresponding on-axis profile of the density (magenta) along with the intensity profile (blue) is shown in (b). (c) – Axial profiles of the relativistic factor, γ (green), the square of the longitudinal momentum, p_z^2 (magenta), and the square of the amplitude of the laser vector potential $|A|^2$, (blue).

#1991 - $15.00 US
Received December 23, 2002; Revised February 04, 2003

Self-focusing in our case is a result of the nonlinear changes in the refractive index, $n_{ref} = [1 - n/(n_c\gamma)]^{1/2}$, induced by the laser pulse through the relativistic mass increase and through the ponderomotively driven electron density perturbation. Initially, when the pulse enters the plasma the relativistic mass increase of the electrons results from their quiver motion in the laser field. However, later on the ponderomotively driven longitudinal electron motion becomes highly relativistic also within the focal region. Thus, the ponderomotive effect also contributes to the relativistic increase in electron mass. Virtually the transverse and longitudinal motions are coupled through the γ factor. As to the electron density perturbation, its effect is to decrease (increase) n_{ref} at the leading (trailing) edge. Indeed, the electron density compression shown in Figs. 3(a) and 3(b) acts as a diverging lens diffracting the relatively low intensity part of the pulse's leading edge. It is created by the front of the pulse, which ponderomotively "snowplows" plasma electrons forward. However, the effect of the density compression is counterbalanced by the relativistic factor in the body of the leading half of the pulse and the net effect is a local increase of the on axis value of the refractive index relative to its off-axis value. This light-induced "lensing" effectively counterbalances the diffractive spreading and the pulse self-focuses.

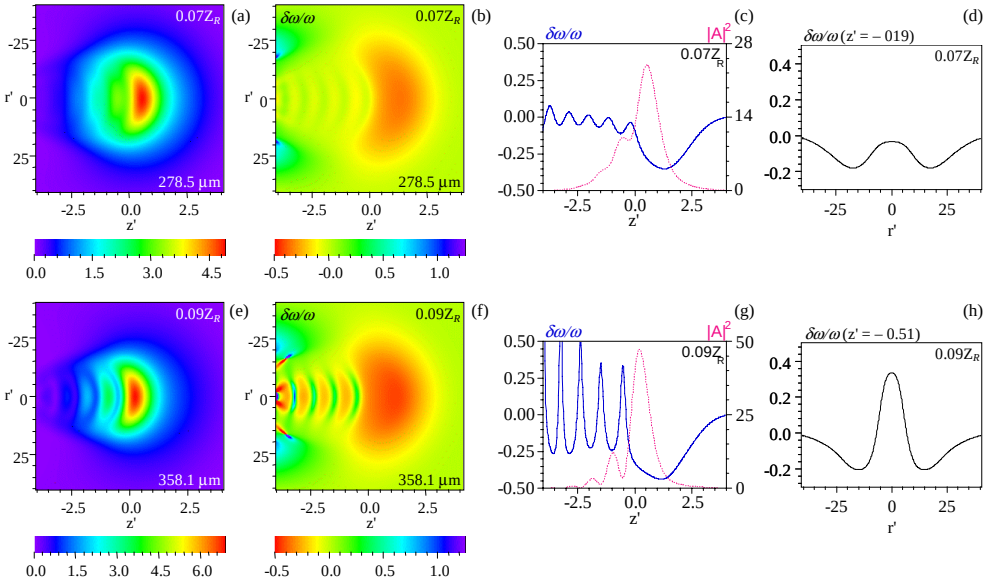

Fig. 4. The contour plots of the laser amplitude $|A|$, (a, e), and of the frequency shift $\delta\omega$ (normalized to the central laser frequency) (b, f), are shown for two propagation distances. Note the large red shifted regions at the front of the pulse as well as the modulated frequency shifts at the trailing edge. (c) and (g) show the corresponding axial profiles of $\delta\omega$ (blue) along with the laser intensity profiles (magenta). (d) and (h) show the radial variations of the frequency shifts, which typically develop at the back of the pulse.

The variations of the effective refractive index along the pulse are responsible for axial modulations of the phase and, respectively, frequency shifts accumulated due to self-phase modulation (SPM) in the course of the pulse propagation. The simulation results presented in Figs. 4(a)-(h) show the evolution of the amplitude $|A|$ and phase ϕ (the latter is presented through the corresponding frequency shift, $\delta\omega = -\partial\phi/\partial\tau$) of the complex envelope $A = |A|\exp(i\phi)$ of the laser pulse for two propagation distances. This numerical full-

#1991 - $15.00 US
Received December 23, 2002; Revised February 04, 2003

field(amplitude + phase) analysis, in analogy with the frequency-resolved optical gating [21], elucidates the role of dispersion as well as of coupling of temporal and spatial evolution of the ultrashort pulse. These figures show contour maps of the frequency shift ("chirp") and their axial and radial profiles together with the corresponding amplitude maps for two propagation distances. The large areas with the red-shifted frequency ($\delta\omega < 0$) are shown in Figs. 4(b) and 4(f). This frequency downshift is located mainly at the leading half of the pulse with a minimum before the main peak. This downshift becomes deeper with time that is also clearly indicated in the axial profiles of the frequency chirp in Figs. 4(c) and 4(g), where they are shown along with the pulse intensity profiles. The longitudinal (time) and radial variations of the frequency shift reflects the complex interplay between the relativistic and ponderomotive effects contributing to the nonlinear index of refraction, which through SPM originates these frequency modulations. First note that the relativistic factor, γ, which is dominant in the shaping of the refractive index, exhibits clearly pronounced longitudinal asymmetry. Figure 3(c) shows the longitudinal profile of γ with the profiles of its ingredients p_z^2 and $|A|^2$. The origin of the asymmetric longitudinal profile of γ, hence that of n_{ref}, is the longitudinal relativistic motion of the plasma electrons, ponderomotively driven by the pulse forward and backward from the focal region as is seen from Fig. 3(c). This asymmetry becomes evident at early stages of the propagation before the time profile modulations at the trailing edge become noticeable. Respectively, we observe an asymmetric broadening of the spectrum: the frequency downshift at the leading half is not followed by symmetric upshift at the trailing half, as one would expect if there were no strongly relativistic plasma response [10,22]. The process of the downshift of the "average" frequency and of the frequency spectral broadening during the propagation of a one-dimensional laser pulse in an underdense plasma have been pointed out and analyzed in [14]. The modulations of the frequency chirp at the back of the pulse appear at a later stage and are steadily enhanced with the accompanying envelope modulations. This enhancement is well seen from Figs. 4(c) and 4(g). Initially small-amplitude undulations start to develop near the peak of the pulse. Then they propagate downhill the back slope. The accompanying phase shifts are affected in such a way that within the regions with higher amplitude the frequency is downshifted, whereas it is upshifted in the regions with lower amplitudes. Arranged in this way, the amplitude and frequency modulations enhance each other and the process turns out to be unstable and it proceeds until the back of the pulse is split into several successive pulses. This development is a result of the FOD effect. The FOD modulates phase shifts, i.e., the frequency spectrum, and through it the envelope time profile. Indeed, direct numerical simulations have shown that without the second term in Eq. (3) accounting for FOD, there is no modulation of frequency shifts and, consequently, there is no splitting of the pulse [16].

A characteristic concave (in the (z', r') plane) shape acquired by the back of the main pulse as well as by the split pulses shown in Figs. 1(d)-1(f), 4(e) correlates with typical radial distribution of the frequency chirp shown in Figs 4(d) and 4(h). Note that in Fig. 4(d) the frequency in the center is upshifted only relatively to the off-axis spectrum, whereas in Fig. 4(h) this difference becomes "absolute" with blue-shifted ($\delta\omega > 0$) spectrum at the center and red-shifted one ($\delta\omega < 0$) off-axis. These transverse modulations of the frequency chirp also are attributed to the FOD effect. On the other hand, under anomalous GVD the blue-shifted parts of the pulse acquire higher group velocities than that of the red-shifted parts. Thus the combined action of GVD, FOD and SPM not only affect the time (longitudinal) profile of the pulse) by SC and by splitting of the pulse, but it also initiates an axial transport of energy, which changes its radial profile.

#1991 - $15.00 US Received December 23, 2002; Revised February 04, 2003

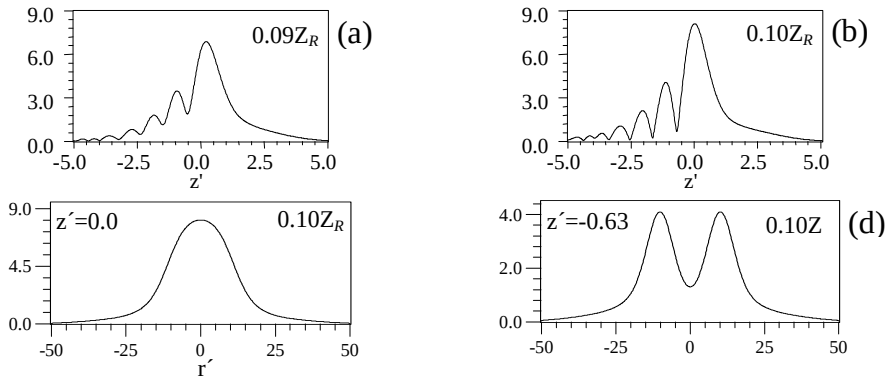

Fig. 5. Modulations of the pulse's temporal profile for two subsequent propagation distances (a, b). The pulse's head self-focuses with a conventional bell-shaped radial profile (c), while its trailing half develops a radial pattern with minimum intensity at the center surrounded by a ring in which the intensity is concentrated (d).

Figures 5 (a) and (b) show the longitudinal profiles of the pulse amplitude for two different propagation distances. The developing modulation of the time envelope and its successive splitting into sequence of pulses are evident. Figures 5 (c) and (d) show the radial profiles of the pulse at its leading and trailing edges, respectively. As it is evident from Fig. 5(d) at the trailing half of the pulse its radial profile has developed a pattern with a radial symmetry of higher order than that of the initial Gaussian profile. Note that, within the conventional paraxial wave equation, a radial transport of energy connected to SF cannot initiate changes in the radial pattern of a laser beam like one observed here [9,12].

After traveling through the plasma a distance much larger than its initial length the pulse as a whole develops a longitudinal scale comparable to the transverse one. This is the evidence that we enter a parameter regime beyond the validity of our model for ultrashort pulses ($\ell_{\mathrm{L}} << \ell_{\perp}$). Therefore the further development is only of mathematical value.

4. Conclusion

In conclusion, we have studied numerically the dynamics of an ultrashort, high peak power, relativistic laser pulse propagating in an underdense plasma. Our numerical simulations are based on a model, which incorporates (i) all relevant finite-pulse-length effects, and (ii) describes laser plasma interactions within a strongly nonlinear, fully relativistic regime. The numerical studies have revealed the importance of these two factors in the evolution of a femtosecond-scale, multiterawatt, high-intensity laser pulse in underdense plasmas. Entering the plasma the pulse initiates large nonlinear changes in the refractive index. These changes are caused by the relativistic and ponderomotive effects, which contribute equally in the regime of strong coupling between the laser and the plasma response. The enhanced SPM in the presence of the GVD effect creates favorable conditions for the pulse SC, which goes synchronously with its SF. Both effects lead to a concentration of the pulse energy with a high rate. However the conventional patterns of SF and SC become significantly modified when with the further reduction of the pulse's longitudinal dimensions the finite-pulse-length effects start to dominate in its evolution. Analyzing the evolution of the SPM induced frequency shifts together with the pulse envelope evolution it was shown that the FOD effect modulates the frequency chirp at the trailing half of the pulse. Coupled with the amplitude modulations, this process develops as an unstable backward propagating perturbation, leading to the splitting of the back of the pulse into a sequence of pulses. The combined effect of GVD, FOD and SPM actively reshapes not only the pulse's time profile, but also its radial profile through the axial redistribution of the pulse energy. As a result the initially Gaussian

#1991 - $15.00 US Received December 23, 2002; Revised February 04, 2003

radial profile during the SF changes to a profile with a higher order of radial symmetry with a ring shaped intensity distribution in the transverse plane. All these clearly show the role of dispersion effects and SPM in the evolution of ultrashort pulses in underdense plasmas. The importance of the detailed studies of these effects for intense laser-matter interactions is evident taking into account that such pulses usually have associated amplified spontaneous emission and pre- (and post) pulses. They create a low-density plasma in front of the main pulse. Thus an ultrashort pulse does propagate through underdense plasmas before reaching the main target. On the other hand, as we have shown, underdense plasma through its large and low-inertia electron nonlinearities is a medium in which an ultrashort, intense laser pulse undergoes violent changes of its temporal, spatial and spectral characteristics. Consequently these changes can significantly alter the laser-matter interactions [5,22]. Therefore detailed characterization of the self-effects governing the ultrashort pulse evolution in underdense plasmas becomes of primary interest for controlling and optimizing the spatial and temporal shape and phase of a laser pulse to improve its delivery to the target with high efficiency.

Acknowledgments

I. G. M. gratefully acknowledges the hospitality of the Istituto di Fisica del Plasma - CNR Milano, and Rainer Exner and Bärbel Exner for their invaluable support of his work.

#1991 - $15.00 US Received December 23, 2002; Revised February 04, 2003